Stress-Strain Characterization of a Dynamically-Controlled Cardiac Phantom with Fluid and Structural Dynamics

Nicolas Charalambous[1], Kristis Michaelides[1], Elias Psimolofitis[2], Vasilis Tzangarakis[3], Demos Michaelides[3], Stelios Angeli[4], and Christakis Constantinides[4]
[1]Hydrus Ltd, Limassol, Cyprus, [2]CNE Limited, Nicosia, Cyprus, [3]α-Evresis Diagnostic Center, Nicosia, Cyprus, [4]U. of Cyprus, Nicosia, Cyprus

Introduction: Myocardial tissue characterization, pre- and post-cellular implantation or following therapy, has become an active area in clinical practice and basic science work. Prior efforts have focused on the invasive [1] and non-invasive MRI characterization of the left ventricular (LV) muscle elasticity [2] to document energetic status, and rates and extent of filling and relaxation [3,4]. Diastolic filling, in particular, is regarded as the outcome of myocardial re-lengthening post-contraction and ventricular flow. The pressure fields developed within the ventricular cavity are the determinants of wall stress and the transmural strain gradients. The temporal evolution of such transmural stress and strain gradients are therefore direct manifestations of structure-function, the muscle's material properties, the active and passive fiber force generation, intra-cavity blood pressure changes and their effects on the endocardial wall [5]. This work develops a methodology for computational modeling, and estimation of global cardiac stress and strain fields of an elastomeric heart of a dynamically controlled cardiac phantom using ex-vivo testing, ^{1}H MRI, and computational fluid dynamics (CFD). The results are compared using the solutions of the Navier-Stokes (NS) equations for the flow velocity fields, in association with bench experimentation and phase contrast (PC) MRI. **Methods:** Cardiac Phantom MRI: A commercially available pneumatic human heart phantom was used (Shelley Medical Imaging Technologies, Canada) in a 10 L water container, and a polyvinyl acetate (PVA) synthetic heart that matches the cardiac ventricular anatomy. The computer-controlled system (Pneumatics Heart Control, Shelley Medical) allows adjustment of heart rates (10-100 bpm) and compression and stretching (based on a maximum driving shaft extension of 2.8 cm, and a maximum torsion of 41^o), achieved with generated motion waveforms. Electrical activity (with external trigger devices) can synchronize acquisitions to the cardiac cycle. Pulsatile fluid flow was ensured through circulation of water through the two-chambered artificial heart. Imaging was performed on a 1.5T scanner (Excelart Atlas, Toshiba) using a FFE-SSFP cardiac imaging sequence and a 32-loop phased array coil, throughout the cardiac cycle. The imaging acquisition parameters were: TE=1.6/5 ms, TR=3.2/10.5 ms, slice thickness (ST)=8 mm, FOV=35/30 cm, BW=±1302 kHz, flip angle=70^o, 128×256 matrix, and 20 short-axis slices. Fifteen phases of the cardiac cycle were acquired at a temporal resolution of 87 ms and spatial resolution of 1.4×2.7×8 mm^3. Cardiac gating was achieved with the scanner's peripheral gating module and an ECG simulator set to a Heart Rate [HR]= 69 bpm. Cardiac Phantom Phase Contrast: PC imaging was also conducted (under the same conditions as listed above) with a conventional PSMRA flow encoding pulse sequence on the 1.5T scanner with v_{enc}=75 cm/s. Reconstructed phase images were analyzed for velocity and flow estimation using ROI analyses with the QFlow software (Medis Medical Imaging, The Netherlands). Flow Validation Study: A flow validation study was conducted using the same flow-phase pulse sequence and analysis methodology, with laminar flows in 1 inch tubing, attained with a water pump (Pentax PM45, Italy) at two different flow settings (25.9 and 26.7 L/min). Inline flows were recorded with a real-time flowmeter (DigiFlow 6710M-66, Savant Electronics, Taiwan). The knee coil was used for multi-axial imaging due to its homogenous B_1-field response. Epicardial Hydrostatic and Chamber Pressure Variation: A Millar catheter (SPR839, Millar Instruments Inc., TX, USA) was positioned at the four inlet/outlet tubing-ventricular chamber interfaces of the heart during motion, and pressure recordings were collected over 10 cardiac cycles. The Millar catheter was attached to an eight channel recording device (ADI Inc., USA), and interfaced with a pressure transducer measuring module, and controlled via the dedicated software PVAN. Inflow and outflow port locations and developed pressures were used to initialize the boundary conditions for CFD simulations. Elastomer Characterization**:** A rectangular PVA sample (Shelley Medical) (11.3×10.64×3.99 mm^3 [length×width×thickness]) was also tested on a universal testing machine (UTM). The sample was subjected to 10 loading cycles of 11 mm extension, requiring a force of 3 N over a 12 second cycle duration. Epicardial Displacement and Strain Estimation: Clusters of three epicardial pin markers were placed on the upper phantom surface in almost equi-planar basal, middle, and apical regions, and the phantom was operated on the bench under the same experimental conditions as those during imaging. Video capture with a digital camera (DCR-TRV22E, Sony, Tokyo, Japan, with a frame rate=30 fps) allowed tracking of the pin-heads during the cardiac cycle and computation of the longitudinal and circumferential epicardial displacements using Matlab. Pin-head tracking and strain tensor formulation was achieved according to Omens et al. [6]. MRI Model Development: The cardiac phantom MR images were imported into ImageJ (NIH, USA) where segmentation allowed the extraction of binary masks of the ventricular elastomer. Masks were processed according to methodology published earlier [7]. CFD Modeling and Stress and Strain Estimation: Imported models in ANSYS (Ansys, USA) facilitated extraction of morphology, definition of material and boundary properties (inertial force, hydrostatic and initial inflow/outflow pressure conditions). Imported material properties closely matched the *ex-vivo* PVA UTM tests. To simulate flow into the LV and RV pools, the NS equations for the fluid flow (non-turbulent Newtonian fluid) [8] were solved on the end-diastolic (ED) and end-systolic (ES) geometries. The constructed mesh was an unstructured mixed element grid composed of hexahedral and tetrahedral elements, wedges and pyramids. An empirical mesh size optimization (coarse and fine meshes) led to a final mesh choice containing >100k elements for each ventricular chamber, sufficient for a mesh-independent simulation. Flow properties were assumed constant over a single cardiac phase. Ventricular pool simulation CFD results were then propagated as initial boundary conditions for the solution of the corresponding cardiac phase for the structural model. To ensure accuracy of the constructed model, imported material properties matched the ex-vivo UTM tests, according to a fitted 2nd order Ogden constitutive model, assuming an incompressible material, according to a strain energy potential $W=\Sigma_i^N[\mu_i/\alpha_i.(\lambda_1^{\alpha i}+\lambda_2^{\alpha i}-2)]$, where λ_i are the principle stretches of the left Cauchy-Green tensor, and μ_i and α_i are material constants determined to be 991,900 and 10,11.1, respectively. **Results and Discussion:** Figure 1 depicts the structural MRI (in long and short axis views), the PC-MRI of a mid-ventricular slice, and the corresponding PC-MRI of the ventricular inlet/outlet ports. The material incompressibility assumption was confirmed from volume curves based on CINE-MRI. Pressure recordings indicated that both tubes of each ventricular chamber allow water inflow or outflow during the cardiac cycle, simulated in an open boundary mode setting. Maximum inflow velocities for RV and LV reached inlet values of 1.4−5.9 cm/s and outlet pressures of -2.5−9.0 mmHg at ED, and corresponding values of 5.7−11.4 cm/s and 1.9−11.5 mmHg at ES, respectively. Flow validation experiments yielded phase images that resulted in estimated flows of 26.1±0.2 (mean±sd) and 27.2±0.3 L/min for the two settings, respectively, resulting in an estimated error of < 2%. Estimated ED and ES ε_{11} strains (Fig. 1) ranged from ±15-20% (MRI) and -8.4−15.6% (CFD). Stress and strain distributions from model computations are shown in Fig. 2.Tabulated are also comparisons of PC-MRI and CFD estimations of mean LV velocities at basal, mid-, and apical levels. Presented results guarantee further computational work using dynamic modeling and validation comparisons between CFD and MRI.

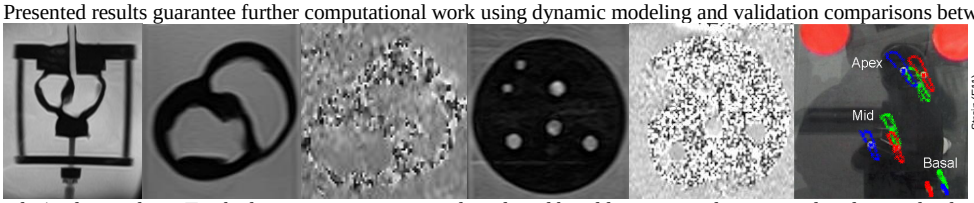

Fig. 1: (Left to right) FFE-SSFP long- and short-axis MRI of the elastomeric human heart and corresponding PC MRI; ^{1}H and PC MRI of the four ventricular pool inlet/outlet conduits; Tracked pin trajectories at apical, mid- and basal locations and corresponding longitudinal strain (ε_{11}) over multiple cardiac cycles.

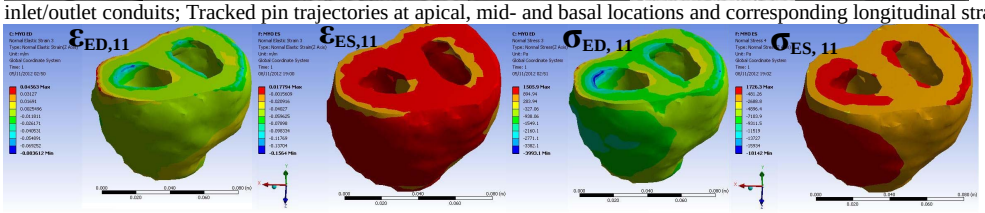

Mean Velocity - Cardiac Location (cm/s)		Cardiac Phase ED	Cardiac Phase ES
BASE	Computational (v_{xyz})	0.8	2.1
	PC-MRI (v_{xy})	1.1	0.8
MID	Computational (v_{xyz})	1.1	5.3
	PC-MRI (v_{xy})	1.8	1.3
APEX	Computational (v_{xyz})	4.0	8.0
	PC-MRI (v_{xy})	0.6	3.1

Fig 3: (Left to right) Elastic strain (ε) and stress (σ) distributions for ED and ES; **Table 1:** 3D and in-plane velocities at ED and ES, estimated using CFD and PC MRI.

References: 1) Stuyvers BDMY, *et. al*. J Phys Lond 502:661-677, 1997; **2)** Kolinpaka MRM 64(3):862-70, 2010; **3)** Aletras A, *et. al*. J. Magn. Reson. 137:247-252, 1999; **4)** Wen H, *et. al*. MRM 54:538-548, 2005; **5)** Hu Z, *et. al*. Med. Image Analysis 7:435-444, 2003; **6)** Omens JH *et al.* Circ. Res. 66:37-45. 1990; **7)** Perperidis D *et al.* CMIG, 36:119-129, 2012; **8)** Thompson R, McVeigh R. MRM. 49:1056-1066, 2003. **Acknowledgements:** Support was received (PI: CC) from grant IPE/TEXNOLOGIA/MHXAN/0609(BE)/05 from the Research Promotion Foundation in Cyprus.